COMPDYN 2011
III ECCOMAS Thematic Conference on
Computational Methods in Structural Dynamics and Earthquake Engineering
M. Papadrakakis, M. Fragiadakis, V. Plevris (eds.)
Corfu, Greece, 25–28 May 2011

NONLINEAR MODELING AND ANALYSIS OF R.C. SPATIAL FRAMES TO STUDY THE EFFECTS OF THE VERTICAL COMPONENT OF NEAR-FAULT GROUND MOTIONS

F. Mazza[1] and M. Mazza[2]

[1] Department of Engineering Modeling, University of Calabria
87036, Rende (Cosenza), Italy
e-mail: fabio.mazza@unical.it

[2] Department of Engineering Modeling, University of Calabria
87036, Rende (Cosenza), Italy
e-mail: mirko.mazza@unical.it

Keywords: R.C. Spatial Frames, Lumped Plasticity Model, Axial Load-Biaxial Bending, Nonlinear Dynamic Analysis, Near-Fault Ground Motions.

Abstract. *Near-fault ground motions are characterized by high values of the ratio α_{PGA} between the peak value of the vertical acceleration, PGA_V, and the analogous value of the horizontal acceleration, PGA_H, which can notably modify the axial force demand in columns (e.g. producing both tension and high compressive forces larger than the balanced force) and the bending moment demand in girders (e.g. plastic hinges are expected along the span of r.c. girders, especially in the upper storeys). At present, the Italian seismic code (NTC08) does not consider the effects of near-fault ground motions in the design of a r.c. framed structure. In order to check the effectiveness of current code provisions, six- and twelve-storey r.c. spatial framed structures are designed according to the provisions of NTC08, considering the horizontal seismic loads acting alone or in combination with the vertical ones. A numerical investigation is carried out considering the nonlinear response of the test structures subjected to horizontal and vertical accelerograms, representative of near-fault ground motions with different values of the acceleration ratio α_{PGA}. A lumped plasticity model (LPM) based on the Haar-Kàrmàn principle is proposed to model the inelastic behaviour of the r.c. frame members. Specifically, the lumped plasticity model for a column (LPMC) includes a piecewise linearization of the bounding surface of the axial load-biaxial bending moment elastic domain, at the end sections where inelastic deformations are expected. On the other hand, the lumped plasticity model for a girder (LPMG) takes into account the potential plastic hinges along the span, due to the vertical ground motion, modifying the uniaxial plastic moments of the end-sections and so avoiding the computational effort required by the sub-discretization of the frame member.*

1 INTRODUCTION

Structural damage of reinforced concrete (r.c.) framed buildings, designed according to recent seismic codes and located in a near-fault area, has been observed during near-fault ground motions [1] and experimentally verified [2]. Generally, the design provisions of current seismic codes are not very accurate for assessing near-fault effects, because only far-fault ground motions are considered. At present, the Italian [3] and European [4] seismic codes do not consider the effects of the vertical component of near-fault ground motions in the design of a r.c. framed structure. These motions are characterized by high values of the ratio between the peak value of the vertical acceleration (PGA_V) and the analogous value of the horizontal acceleration (PGA_H) [5]. More specifically, high values of the acceleration ratio α_{PGA} can notably modify the axial load in r.c. columns, producing undesirable phenomena in these elements [6]: e.g., reduction in the shear capacity, buckling of the longitudinal bars, brittle failure in compression, bond deterioration or failure under tension. Moreover, plastic hinges are expected along the span of the girders, especially if rather long [7], and in the upper storeys, where the effects of the gravity loads generally prevail over those of the horizontal seismic loads and an amplification of the vertical motion is expected [8].

In order to establish if suitable additional code guidelines are needed, it is very important to study the nonlinear response of r.c. spatial frames subjected to near-fault ground motions. The high computational effort required to obtain accurate results by finite elements or fibre models has encouraged the development of simplified approaches [9]. In the present work, a lumped plasticity model (LPM) based on the Haar-Kàrmàn principle is proposed to model the inelastic behaviour of r.c. frame members. Specifically, the lumped plasticity model for a r.c. column (LPMC) includes a piecewise linearization of the bounding surface of the axial load-biaxial bending moment elastic domain, at the end sections where inelastic deformations are expected. Each flat surface corresponds to a plastic strain mechanism for the section, defined by axial strains and curvatures. This type of element represents a good choice for the response simulation of structural members, like columns, that may experience inelastic deformations at the end sections. On the contrary, the lumped plasticity model for a r.c. girder (LPMG) takes into account the potential plastic hinges along the span of the girders, due to the vertical ground motion, modifying the uniaxial plastic moments of the end-sections depending on the top and bottom plastic moments of selected critical intermediate sections and so avoiding the computational effort required by the sub-discretization of the frame member [10].

Six- and twelve-storey r.c. spatial frames are assumed as test structures and designed according to the provisions of the Italian seismic code (NTC08) considering (besides the gravity loads) the horizontal seismic loads acting alone or in combination with the vertical ones. Horizontal and vertical accelerograms, representative of near-fault ground motions with different values of the acceleration ratio α_{PGA}, are considered for the numerical investigation.

2 LUMPED PLASTICITY MODELING

The nonlinear dynamic analysis of a spatial framed structure can be carried out adopting a numerical step-by-step procedure based on an initial stress-like iterative procedure [11]. At each step of the analysis, the elastic-plastic behaviour of a beam element is described using the Haar-Kàrmàn principle, without satisfying nodal equilibrium conditions, once the initial state and the incremental load in the step are known. Then, an implicit two-parameter integration scheme is adopted in order to satisfy the global dynamic equilibrium of the overall structure. Each frame member is modeled by a LPM composed of two parallel elements, one elastic-perfectly plastic and the other linearly elastic, assuming a bilinear moment-curvature (M-χ) law, depending on the axial load in the case of a column. The elastic component is cha-

racterized by the flexural stiffness pEI, p being the hardening ratio of the (M-χ) law. Torsional strains are assumed to be fully elastic while shear strains are neglected. Distributed masses are considered along the girders to evaluate the influence of the vertical vibrations.

2.1 Frame members in biaxial bending with axial force

The nonlinear behaviour of r.c. structural elements under biaxial bending with axial force is generally based on the knowledge of the bounding surface of the cross-sections, resulting from the plastic moments obtained for different values of the axial force [12]. A lumped plasticity model, labelled as LPMC, is proposed for a r.c. column, assuming that the bounding surface of the elastic domain is described by means of flat surfaces. More specifically, the inelastic deformations, supposed as lumped at the end cross-sections, are represented by the axial strain ε_P, along the longitudinal axis x, and the curvatures χ_{Py} and χ_{Pz}, along the principal axes y and z, collected in the vector

$$\boldsymbol{\varepsilon}_P = \left[\varepsilon_P, \chi_{Py}, \chi_{Pz}\right]^T \tag{1}$$

and referring to the (geometric) centroid of the cross-section. Denoting the corresponding generalized stresses at the end section by the vector

$$\boldsymbol{\sigma} = \left[N, M_y, M_z\right]^T \tag{2}$$

and the plastic stresses, related to $\boldsymbol{\varepsilon}_{Pk}=\boldsymbol{n}_k$, by $\boldsymbol{\sigma}_{Pk}$, the elastic domain $g(\boldsymbol{\sigma})=0$ can be approximated by n_{fs} flat surfaces $g_k(\boldsymbol{\sigma})$, each defined by a different (normal) direction $\boldsymbol{n}_k$.

As suggested in [13], a satisfactory representation of the axial load-biaxial bending moment bounding surface of the elastic domain can be obtained considering 26 flat surfaces, including: 6 surfaces normal to the principal axes x, y and z (Figure 1a); 12 surfaces normal to the bisections of the y-z, x-y and x-z principal planes (Figure 1b); 8 surfaces normal to the bisections of the octants (Figure 1c). The piecewise linearized elastic domain is characterized by the corresponding 26 columns of the matrix

$$\boldsymbol{N} = \begin{bmatrix} 1 & -1 & 0 & 0 & 0 & 0 & 0 & 0 & 0 & 0 & c_{yx} & c_{yx} & -c_{yx} & -c_{yx} & c_{zx} & c_{zx} & -c_{zx} & -c_{zx} \\ 0 & 0 & 1 & -1 & 0 & 0 & 1 & -1 & 1 & -1 & 1 & -1 & 1 & -1 & 0 & 0 & 0 & 0 \\ 0 & 0 & 0 & 0 & 1 & -1 & c_{yz} & c_{yz} & -c_{yz} & -c_{yz} & 0 & 0 & 0 & 0 & 1 & -1 & 1 & -1 \\ c'_{yz} & c'_{yz} & -c'_{yz} & -c'_{yz} & c'_{yz} & c'_{yz} & -c'_{yz} & -c'_{yz} & & & & & & & & & & \\ 1 & -1 & 1 & -1 & 1 & -1 & 1 & -1 & & & & & & & & & & \\ c_{yz} & c_{yz} & c_{yz} & c_{yz} & -c_{yz} & -c_{yz} & -c_{yz} & -c_{yz} & & & & & & & & & & \end{bmatrix} \tag{3}$$

where each column represents a vector $\boldsymbol{n}_k$ defined starting from

$$c_{yx} = \frac{\left\|\boldsymbol{\sigma}_{P3}-\boldsymbol{\sigma}_{P4}\right\|}{\left\|\boldsymbol{\sigma}_{P1}-\boldsymbol{\sigma}_{P2}\right\|}, \quad c_{zx} = \frac{\left\|\boldsymbol{\sigma}_{P5}-\boldsymbol{\sigma}_{P6}\right\|}{\left\|\boldsymbol{\sigma}_{P1}-\boldsymbol{\sigma}_{P2}\right\|}, \quad c_{yz} = \frac{\left\|\boldsymbol{\sigma}_{P3}-\boldsymbol{\sigma}_{P4}\right\|}{\left\|\boldsymbol{\sigma}_{P5}-\boldsymbol{\sigma}_{P6}\right\|}, \quad c'_{yz} = \frac{\left\|\boldsymbol{\sigma}_{P7}-\boldsymbol{\sigma}_{P10}\right\|}{\left\|\boldsymbol{\sigma}_{P1}-\boldsymbol{\sigma}_{P2}\right\|} \tag{4}$$

which refer to the plastic generalized stresses

$$\begin{gathered} \boldsymbol{\sigma}_{P1} = \begin{bmatrix} N_{P1} \\ 0 \\ 0 \end{bmatrix}, \boldsymbol{\sigma}_{P2} = \begin{bmatrix} N_{P2} \\ 0 \\ 0 \end{bmatrix}, \boldsymbol{\sigma}_{P3} = \begin{bmatrix} N_{P3} \\ M_{Py3} \\ 0 \end{bmatrix}, \boldsymbol{\sigma}_{P4} = \begin{bmatrix} N_{P4} \\ M_{Py4} \\ 0 \end{bmatrix}, \boldsymbol{\sigma}_{P5} = \begin{bmatrix} N_{P5} \\ 0 \\ M_{Pz5} \end{bmatrix}, \boldsymbol{\sigma}_{P6} = \begin{bmatrix} N_{P6} \\ 0 \\ M_{Pz6} \end{bmatrix} \\ \boldsymbol{\sigma}_{P7} = \begin{bmatrix} N_{P7} \\ M_{Py7} \\ M_{Pz7} \end{bmatrix}, \boldsymbol{\sigma}_{P8} = \begin{bmatrix} N_{P8} \\ M_{Py8} \\ M_{Pz8} \end{bmatrix}, \boldsymbol{\sigma}_{P9} = \begin{bmatrix} N_{P9} \\ M_{Py9} \\ M_{Pz9} \end{bmatrix}, \boldsymbol{\sigma}_{P10} = \begin{bmatrix} N_{P10} \\ M_{Py10} \\ M_{Pz10} \end{bmatrix} \end{gathered} \tag{5}$$

In particular, once the plastic strain mechanism of the cross-section corresponding to the vector $\boldsymbol{n}_k$ ($k=1..n_{fs}$) is considered, the maximum compressive strain in concrete (ε_{cmax}) and the maximum tensile strain in longitudinal steel reinforcement (ε_{smax}) are evaluated, avoiding values greater than the corresponding ultimate ones (e.g. $\varepsilon_{cu}=0.35\%$ and $\varepsilon_{su}=1\%$). In this way, the position of the neutral axis and the area of the compressed concrete section (A_c) being known, the components of the generalized plastic stress vector $\boldsymbol{\sigma}_{Pk}$ can be evaluated by the equilibrium equations:

$$N_{Pk}=\int_{A_c}\sigma_c dA+\sum_{i=1}^{n_b}A_{si}\sigma_{si},\quad M_{Pyk}=-\int_{A_c}\sigma_c z\,dA-\sum_{i=1}^{n_b}A_{si}\sigma_{si}z_i,\quad M_{Pzk}=\int_{A_c}\sigma_c y\,dA+\sum_{i=1}^{n_b}A_{si}\sigma_{si}y_i \tag{6}$$

where $\sigma_c=\sigma_c(\varepsilon)$ and $\sigma_{si}=\sigma_{si}(\varepsilon)$. In Eq. (5) n_b is the number of longitudinal bars while (y_i, z_i) and A_{si} define, respectively, the position and area of each bar. Elastic-perfectly plastic constitutive laws are assumed for both concrete (σ_c–ε_c) and steel (σ_s–ε_s), assuming stresses and strains with the appropriate signs (i.e. negative for compression and positive for tension).

At each step of the analysis, the elastic-plastic behaviour of a column, once the initial state and the incremental load are known, can be obtained by using the Haar-Kàrmàn principle. It states that, among all the generalized stress fields $\boldsymbol{\sigma}$ satisfying equilibrium, the elastic-plastic solution $\boldsymbol{\sigma}_{EP}$ is that with minimum distance, in terms of complementary energy Π_c, from the elastic solution $\boldsymbol{\sigma}_E$ [11]

$$\Pi_c\left(\boldsymbol{\sigma}_{EP}\right)=\frac{L}{2}\int_0^1\left(\boldsymbol{\sigma}_{EP}-\boldsymbol{\sigma}_E\right)^T\boldsymbol{D}_c^{-1}\left(\boldsymbol{\sigma}_{EP}-\boldsymbol{\sigma}_E\right)d\xi=min. \tag{7}$$

$\xi(=x/L)$ being a nondimensional abscissa, L the length of the beam element and $\boldsymbol{D}_c$ the elastic matrix of a column. The plastic admissibility conditions

$$g_k\left(\boldsymbol{\sigma}_{EP}\right)\le 0\quad \text{for } k=1..n_{fs} \tag{8}$$

also have to be satisfied at the end sections of the beam element. The elastic-plastic solution corresponds to the tangent point between a level curve of $\Pi_c(\boldsymbol{\sigma}_{EP})$ and the piecewise approximation of the bounding surface of the elastic domain. Moreover, when the elastic solution lies within the fan limited by the planes normal to the boundaries of the flat surfaces, the elastic-plastic solution corresponds to a point along the corner line resulting from the intersection between these surfaces.

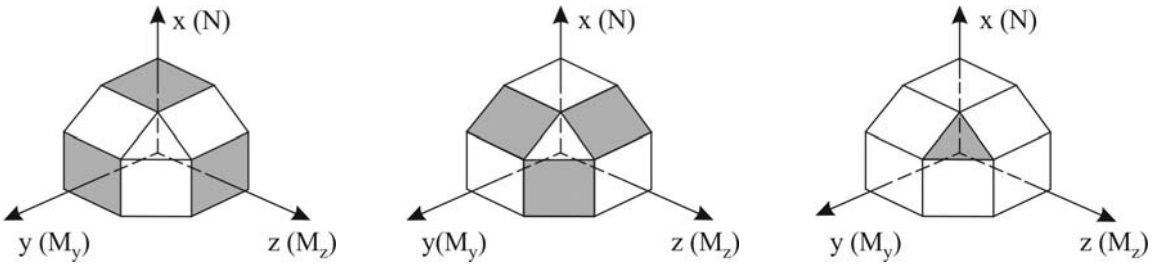

(a) Surfaces normal to the *x*, *y* and *z* axes.

(b) Surfaces normal to the bisections of the *y*-*z*, *x*-*y* and *x*-*z* planes.

Surface normal to the bisection of the octant.

Figure 1: Flat surfaces approximating the elastic domain for the end sections of a column.

2.2 Frame members in uniaxial bending without axial force

A lumped plasticity model, already proposed by the authors [10], is adopted for a r.c. girder and labelled as LPMG. The elastic-plastic solution is evaluated only at the end sections (*i* and *j*) in the vertical plane (i.e. *x*-*z* plane) of bending. Moreover, the potential inelastic de-

formations lumped at n_s intermediate sections along the span, due to the vertical ground motions, are also checked. In order to avoid the computational effort due to the sub-discretization of the frame member, the elastic solution at the end section i (j) is modified taking into account the possible inelastic effects occurring at an intermediate section s ($s=1..\ n_s$), besides those at the end section j (i). Specifically, when a plastic (flexural) distortion

$$\Delta\phi_{Pys} = \Delta M_{EPys}\left(\frac{4EI_y(1-p)}{L}\left(3\left(\frac{x_s}{L}\right)^2 - 3\left(\frac{x_s}{L}\right)+1\right)\right)^{-1} \tag{9}$$

consequent to an elastic-plastic moment M_{EPys} greater than the corresponding plastic moment occurs at an intermediate section of abscissa x_s, the corresponding moments at the end sections can be evaluated as

$$\Delta M_{EPyi}^{(s)} = \frac{2EI_y(1-p)}{L}\left(3\left(\frac{x_s}{L}\right)-2\right)\Delta\phi_{Pys},\quad \Delta M_{EPyj}^{(s)} = \frac{2EI_y(1-p)}{L}\left(3\left(\frac{x_s}{L}\right)-1\right)\Delta\phi_{Pys} \tag{10a,b}$$

With reference to the bending moment along the principal axis y and neglecting the inflection along the principal axis z, the generalized stresses of a girder are denoted by the vector

$$\boldsymbol{\sigma} = \left[M_{yi}, M_{yj}\right]^T \tag{11}$$

Then the elastic-plastic solution satisfying equilibrium is obtained, according to the Haar-Kàrmàn principle, minimizing the complementary energy

$$\Pi_c\left(\boldsymbol{\sigma}_{EP}\right) = \frac{L}{2}\int_0^1 \left(\boldsymbol{\sigma}_{EP} - \boldsymbol{\sigma}_E - \Delta\boldsymbol{\sigma}_{EP}^{(s)}\right)^T \mathbf{D}_g^{-1}\left(\boldsymbol{\sigma}_{EP} - \boldsymbol{\sigma}_E - \Delta\boldsymbol{\sigma}_{EP}^{(s)}\right) d\xi = min. \tag{12}$$

where $\mathbf{D}_g$ is the elastic matrix of a girder. Moreover, the plastic admissibility condition

$$g\left(\boldsymbol{\sigma}_{EP}\right) \le 0 \tag{13}$$

also has to be satisfied at the end sections of the beam element. Specifically, the (uniaxial) top (T) and bottom (B) plastic moments at the end sections

$$\boldsymbol{\sigma}_{P,T} = \left[M_{Pyi,T}, M_{Pyj,T}\right]^T \quad , \quad \boldsymbol{\sigma}_{P,B} = \left[M_{Pyi,B}, M_{Pyj,B}\right]^T \tag{14a,b}$$

are modified during the nonlinear analysis, assuming the following values when a plastic distortion occurs at an intermediate section (see Figure 2)

$$\bar{\boldsymbol{\sigma}}_{P,T} = \left[\bar{M}_{Pyi,T}, \bar{M}_{Pyj,T}\right]^T \quad , \quad \bar{\boldsymbol{\sigma}}_{P,B} = \left[\bar{M}_{Pyi,B}, \bar{M}_{Pyj,B}\right]^T \tag{15a,b}$$

The elastic-plastic solution of the problem defined by the Equations (12) and (13) can be obtained by a predictor-corrector procedure. It is triggered evaluating the elastic-plastic solution at an end section (e.g. end section i) by the formula:

$$M_{EPyi}^{(0)} = max\left(-\bar{M}_{Pyi,T}, min\left(\bar{M}_{Pyi,B}, M_{Eyi} + \sum_{s=1}^{n_s}\Delta M_{EPyi}^{(s)}\right)\right) \tag{16}$$

Afterwards the elastic-plastic solution is alternately evaluated at the end section i (j) and j (i)

$$M_{EPyj}^{(k)} = max\left(-\bar{M}_{Pyj,B}, min\left(\bar{M}_{Pyj,T}, M_{Eyj} + \sum_{s=1}^{n_s}\Delta M_{EPyj}^{(s)} - \frac{M_{Eyi} + \sum_{s=1}^{n_s}\Delta M_{EPyj}^{(s)} - M_{EPyi}^{(k-1)}}{2}\right)\right) \tag{17}$$

$$M_{EPyi}^{(k+1)} = max\left(-\bar{M}_{Pyi,T}, min\left(\bar{M}_{Pyi,B}, M_{Eyi} + \sum_{s=1}^{n_s} \Delta M_{EPyi}^{(s)} - \frac{M_{Eyj} + \sum_{s=1}^{n_s} \Delta M_{EPyi}^{(s)} - M_{EPyj}^{(k)}}{2} \right) \right) \quad (18)$$

In cases where the intermediate sections experience inelastic deformations, Eqns. (17) and (18) are solved iteratively until, in these sections, at the iteration loop k the differences between the plastic moments and the elastic-plastic moments evaluated by the equilibrium, starting from the elastic-plastic solution at the end sections, become less than a prefixed tolerance.

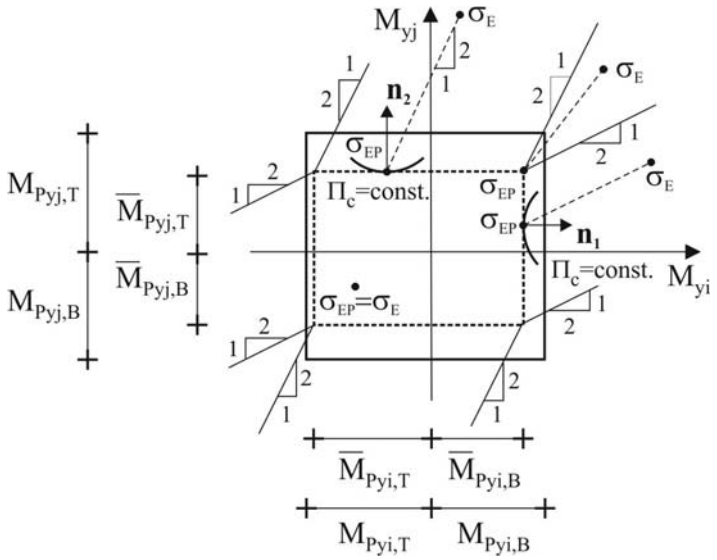

Figure 2: Bounding surface of the elastic domain for the end sections of a girder.

3 LAYOUT AND DESIGN OF THE R.C. FRAMED BUILDINGS

Typical six- and twelve-storey residential buildings with r.c. framed structures, whose symmetric plan is shown in Figure 3, are considered as test structures. Deep girders are placed along the perimeter of the building together with infilled walls assumed as non-structural elements regularly distributed in elevation; deep and flat girders, perpendicular and parallel to the floor slab direction, respectively, are assumed inside the building. Geometric dimensions of the girders and columns are shown in Table 1. Moreover, the vibration periods corresponding to the high-participation modes with prevailing components in the horizontal and vertical directions are: T_{1X}=0.576s, T_{1Y}=0.698s and T_{1Z}=0.064s, for the six-storey buildings; T_{1X}=0.993s, T_{1Y}=1.249s and T_{1Z}=0.103s, for the twelve-storey buildings. The gravity loads used in the design are represented by dead- and live-loads, equal respectively to: 4.8 kN/m^2 and 2 kN/m^2, for the top floor; 5.7 kN/m^2 and 2 kN/m^2, for the other floors. The weight of the perimeter masonry-infills is taken into account considering a gravity load of 2.7 kN/m^2. A cylindrical compressive strength of 25 N/mm^2 for the concrete and a yield strength of 450 N/mm^2 for the steel are considered.

The proportioning of the test structures has been done according to the Italian seismic code (Technical Regulations for Constructions 2008, NTC08 [3]) assuming, besides the gravity loads, the horizontal seismic loads acting alone or in combination with the vertical ones. Each building (B) is identified by two symbols: the first one (6 or 12) indicates the number of storeys, the second one refers to the design seismic loads which are considered (i.e.: H, when considering only the horizontal component of the seismic loads; HV, when also considering

the vertical component of the seismic loads). The following assumptions have been made: medium subsoil (class B, subsoil parameters: S_{SH}=1.13 in the horizontal direction and S_{SV}=1 in the vertical one); flat terrain (class T1, topographic parameter: S_T=1).

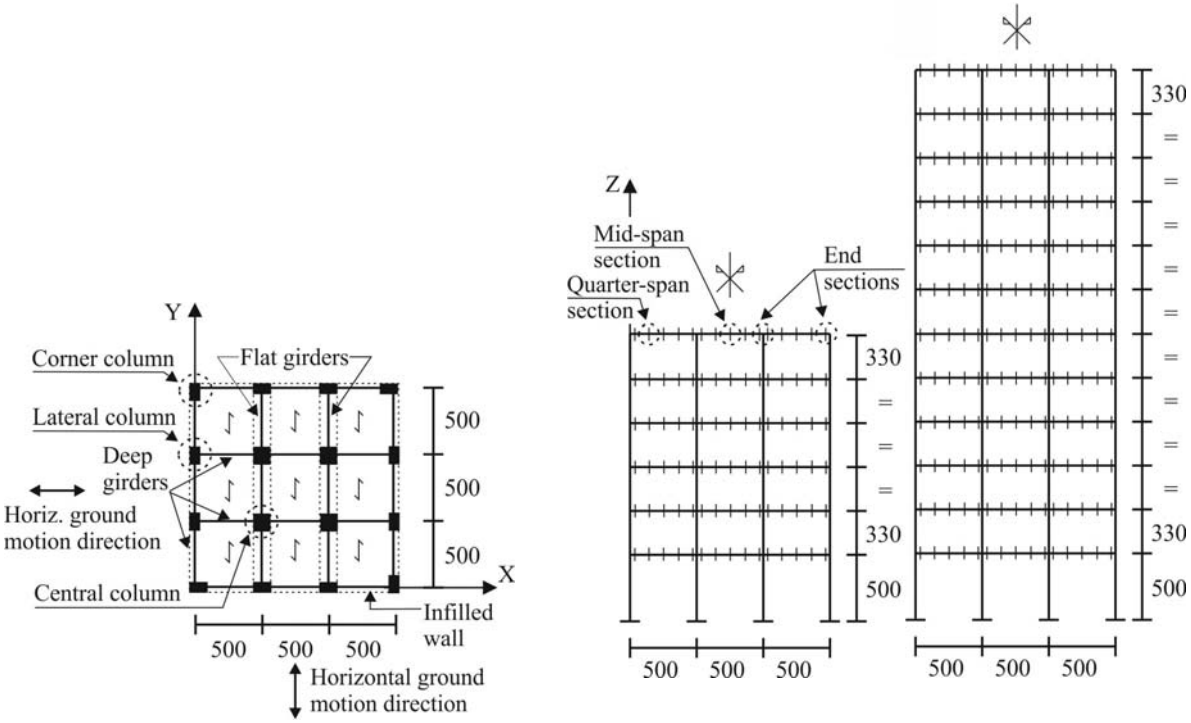

(a) Plan of the buildings. (b) Six-storey frames. (c) Twelve-storey frames.

Figure 3: R.c. test structures (dimensions in cm).

Storey	Corner columns	Lateral columns	Central columns	Deep girders	Flat girders
12	30x30	30x40	40x40	30x50	50x25
11	30x30	30x40	40x40	30x50	50x25
10	30x40	30x50	40x40	30x50	60x25
9	30x40	30x50	40x40	30x60	60x25
8	35x40	35x60	50x50	30x60	70x25
7	35x40	35x60	50x50	30x60	70x25
6	40x50 (30x50)	45x60 (30x50)	60x60 (40x40)	40x65 (30x50)	80x25 (50x25)
5	40x50 (30x50)	45x60 (30x50)	60x60 (40x40)	40x65 (30x50)	80x25 (50x25)
4	50x60 (30x60)	50x70 (40x60)	70x70 (50x50)	40x65 (30x60)	90x25 (60x25)
3	50x60 (30x60)	50x70 (40x60)	70x70 (50x50)	40x70 (30x60)	90x25 (60x25)
2	50x70 (40x70)	50x90 (50x80)	80x80 (60x60)	40x70 (40x60)	100x25 (70x25)
1	50x70 (40x70)	50x90 (50x80)	80x80 (60x60)	40x70 (40x60)	100x25 (70x25)

Table 1: Section dimensions (in cm) of the six- (in brackets) and twelve-storey r.c. buildings.

The design is carried out to comply with the ultimate limit state (ULS) of life safety, according to the horizontal and vertical elastic response spectra whose main data are reported in Table 2: i.e. return period (T_r) corresponding to a nominal life of the structure equal to 50 years; peak ground accelerations in the horizontal (PGA_H) and vertical (PGA_V) directions; amplification factors defining the maximum horizontal (F_o) and vertical (F_v) spectral acceleration on rock-site; upper limit of the period of the constant spectral acceleration branch in the horizontal direction (T^*_C). Six- and twelve-storey structures have to be classified as regular in plan and irregular in elevation, according to the criteria imposed by NTC08. As a consequence, a low ductility class is considered, assuming: behaviour factor for the horizontal seismic loads, q_H=3.12; behaviour factor for the vertical seismic loads, q_V=1.5. Finally, the

serviceability limit state (SLS) of damage is also controlled, checking that, under the horizontal seismic loads corresponding to the elastic response spectra whose main parameters are shown in Table 2, the inter-storey drift is less than 0.5% of the storey height. Detailing for local ductility is also imposed to satisfy minimum conditions for the longitudinal bars of the r.c. frame members. Finally, capacity design rules regarding the beam-column moment ratio and shear forces and local ductility requirement of girders and columns are also satisfied.

Limit state	T_r (years)	PGA_H (g)	PGA_V (g)	F_o	F_v	T^*_C (s)
ULS (Life safety)	475	0.312	0.276	2.44	1.73	0.370
SLS (Damage)	50	0.108	-	2.28	-	0.301

Table 2: Main parameters of the horizontal elastic response spectra.

4 NUMERICAL RESULTS

In order to evaluate the effects produced by the combination of the horizontal and vertical components of near-fault ground motions on the response of r.c. spatial frames, a computer code has been implemented according to the LPMs proposed in Section 2. A bilinear moment-curvature law is adopted, assuming a hardening ratio p=5%. In the Rayleigh hypothesis, the damping matrix is assumed as a linear combination of the mass and stiffness matrices, assuming a viscous damping ratio equal to 5% or 2% with reference to the two vibration periods corresponding to high-participation modes with components prevailing in the Y (T_{1Y}) or Z (T_{1Z}) direction, respectively. In this way, an intermediate value of the damping ratio is achieved in the range of vibration periods T_{1Z}-T_{1Y}, while the higher frequency modes, which do not contribute significantly to the dynamic response, are practically eliminated due to their high damping ratio. Plastic conditions are checked at the end sections of the columns, considering an approximation with flat surfaces of the axial force-biaxial bending moment bounding surface of the elastic domain (see Section 2.1). Three intermediate sections (i.e. the two quarter-span sections and the mid-span section) are checked along the span of the girders, in addition to the end sections (Figure 3b) even if, according to the model proposed in Section 2.2, girders are discretized with only one element instead of four sub-elements, reducing the computational effort of the discretization by about 2/3.

The nonlinear dynamic response of the B6H, B6HV, B12H and B12HV test structures, which are described in Section 3, is studied with reference to the records of the Imperial Valley earthquake, available in the Pacific Earthquake Engineering Research center database [14]. More specifically, ground motions recorded at different stations placed at close range to one another and exhibiting high values of the acceleration ratio α_{PGA}(=PGA_V/PGA_H) are considered. It is worth mentioning that the accelerograms are characterized by a PGA_H value approximately comparable, for one of the two horizontal directions, with the one adopted in the design of the test structures (i.e. PGA_H=0.312g in Table 2). In Table 3 the main data of the selected near-fault ground motions are reported: recording station, closest distance to fault rupture (D); magnitude (M_s), peak ground acceleration for the horizontal components ($PGA_{H,1}$ and $PGA_{H,2}$) and the vertical one (PGA_V) and acceleration ratios ($\alpha_{PGA,1}$ and $\alpha_{PGA,2}$). As can be observed, α_{PGA} has a maximum value of 2.009 for the El Centro Differential Array (D.A.) station as opposed to the value 1.13 prescribed by NTC08 in the examined case (see Table 2).

Station	D	M_s	$PGA_{H,1}$	$PGA_{H,2}$	PGA_V	$\alpha_{PGA,1}$	$\alpha_{PGA,2}$
El Centro Array #5	1.0 km	6.9	0.379g	0.519g	0.537g	1.417	1.035
El Centro Array #7	0.6 km	6.9	0.338g	0.463g	0.544g	1.609	1.175
El Centro Differential Array	5.3 km	6.9	0.352g	0.480g	0.707g	2.009	1.473

Table 3: Main data of the selected near-fault ground motions (Imperial Valley, 15/10/1979).

The elastic (normalized) response spectra of acceleration in the horizontal ($S_{aH,1}$ and $S_{aH,2}$) and vertical (S_{aV}) directions are plotted in Figure 4, assuming an equivalent viscous damping ratio in the horizontal direction, ξ_H, equal to 5%, and an analogous ratio in the vertical direction, ξ_V, equal to 2% due to the low damping capacity of the structure expected in this direction [1]. The response spectra of these motions are compared with the corresponding target NTC08 response spectra for a high-risk seismic region and a medium subsoil class (class B): i.e. PGA_H=0.312g and PGA_V=0.276g. It is interesting to note that in the vertical direction the spectral values for the El Centro ground motions (Figure 4c) are much greater than those corresponding to NTC08, at least in the range of the vibration periods which are more relevant for the test structures.

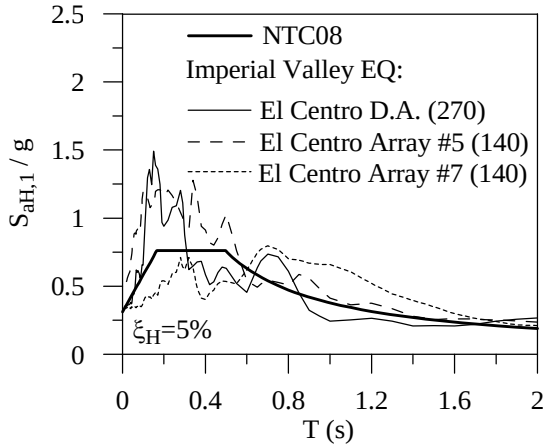

(a) Horizontal direction No. 1.

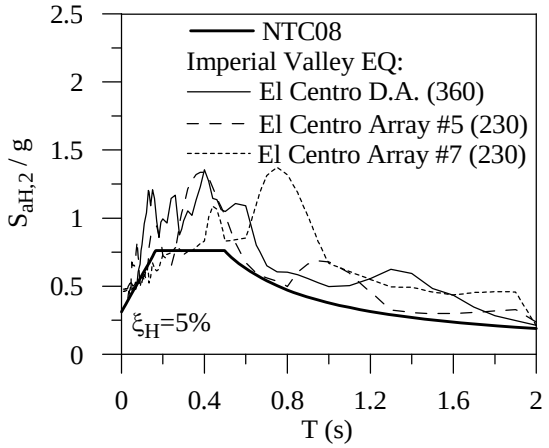

(b) Horizontal direction No. 2.

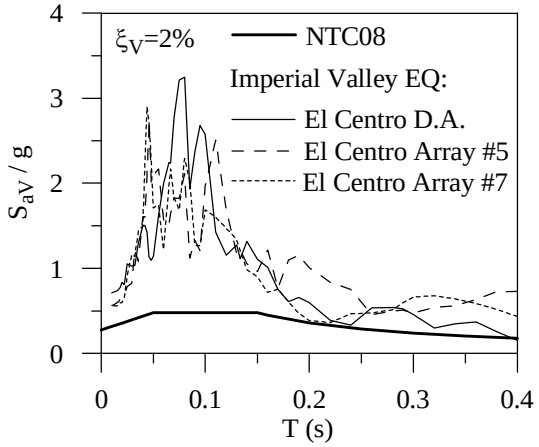

(c) Vertical direction.

Figure 4: Acceleration (elastic) response spectra.

To emphasize the importance of also considering the vertical ground motion, the main response parameters affected by this component are considered: i.e. curvature ductility demand at the potentially critical sections (i.e. end, quarter span and mid-span sections) of the girders, for each of the two loading directions; curvature ductility demand, at the end sections, and axial force demand for the columns. More specifically, the ductility demand for a column is evaluated with reference to the radial direction defined by the bending moment axis vector

$$\mu_{max,r} = \frac{\chi_{max,r}}{\chi_{Er}} = \frac{\sqrt{\left(\chi_{Ey} + \Sigma\,\Delta\chi_{Py}\right)^2 + \left(\chi_{Ez} + \Sigma\,\Delta\chi_{Pz}\right)^2}}{M_{Pr}\left[N_V\right]/\left(EI_r\right)} \tag{19}$$

where $\chi_{max,r}$ and $\chi_{E,r}$ represent the maximum and yielding curvatures, respectively, in the radial direction. Plastic curvatures at each step of the analysis (i.e. $\Delta\chi_{Py}$ and $\Delta\chi_{Pz}$) are accumulated and added to the yielding curvatures at the current step (i.e. χ_{Ey} and χ_{Ez}). Finally, the plastic moment (M_{Pr}) is calculated considering the axial force due to the gravity loads only (N_V) and referring to the radial direction identified by $\chi_{max,r}$.

In order to compare the response of the test structures designed for the horizontal seismic loads only (i.e. B6H and B12H structures) with that of the analogous structures designed also for the vertical seismic loads (i.e. B6HV and B12HV structures), the mean values of the ductility demand of girders and columns are reported in Figures 5 and 6. The results below were obtained as an average of the maximum (local) curvature ductility demand attained at the most critical sections of the structures subjected to the selected Imperial Valley ground motions (see Table 3). The numerical investigation is carried out considering the horizontal components of motion acting alone (H), for B6H and B12H structures, or contemporaneously with the corresponding vertical component (H+V), for B6HV and B12HV structures. Moreover, the horizontal accelerogram with $PGA_{H,1}$ ($PGA_{H,2}$) is applied twice, once along the principal axis X (Y) and the other along the principal axis Y (X) of the building plan.

The curves in Figures 5a and 6a correspond to the mean ductility demand for the end sections and quarter-span sections of the interior deep girders, perpendicular to the floor slab direction shown in Figure 3a. As shown, the effects of the vertical component of ECDA, ECA#5 and ECA#7 ground motions proved to be more evident at the upper floors where bending moments due to vertical seismic loads are more important than those due to the horizontal seismic loads. More specifically, the end sections, at the top side, and quarter-span sections, at the bottom one, proved to be the more stressed sections. This kind of behaviour can be explained observing that the ductility demand at these sections, in contrast to the mid-span ones, already appears under the horizontal components of the Imperial Valley ground motions. Moreover, the bottom plastic moments of the quarter-span sections, at the upper floors, were less than or equal to those assumed at the mid-span sections. This result emphasizes the need to take into account the vertical ground motion in the design of the girders, especially at the upper storeys. Further results, omitted for the sake of brevity, highlighted that flat girders, parallel to the floor slab direction, exhibit plastic deformations at the end sections due to the horizontal components of the ground motion, but the intermediate sections are practically independent of the vertical component due to their small tributary mass.

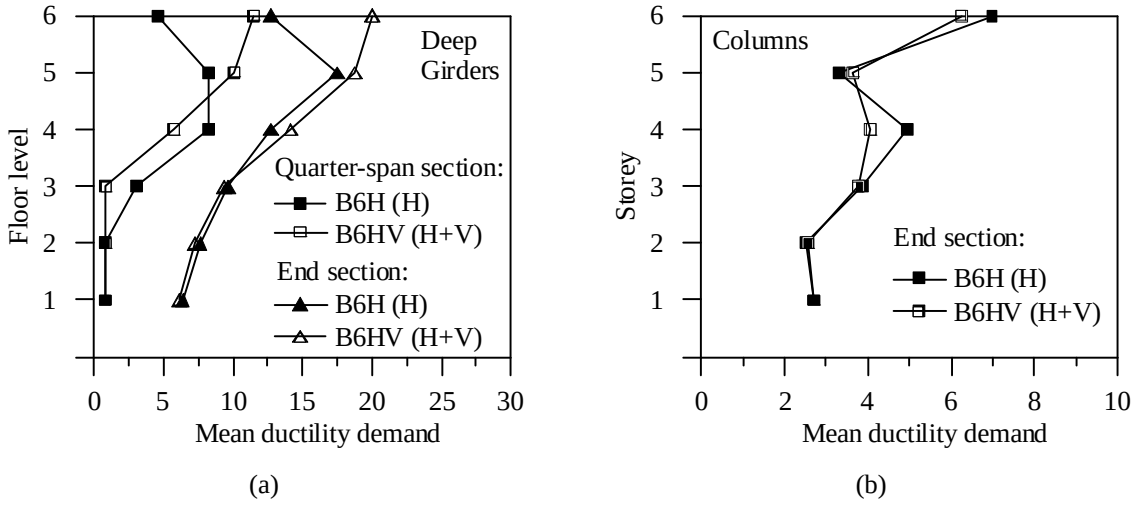

Figure 5: Mean ductility demand of B6H and B6HV structures subjected, respectively, to the horizontal components (H) and horizontal and vertical components (H+V) of the Imperial Valley earthquakes.

Successively, the maximum values of the mean ductility demand at the end sections of the columns are evaluated with reference to the same cases as discussed above. As can be observed, the effects of the vertical ground motion are negligible for the B6HV structure (Figure 5b) and generally limited to the upper storeys for the B12HV structure (Figure 6b). However, note that the mean ductility demand at each storey is shown for the (central, lateral or corner) column section exhibiting the maximum value, but in many cases the section where the maximum ductility value is attained is different, when the horizontal ground motions alone (H) or in combination with the vertical ground motion (H+V) are considered. As expected, a "strong-column weak-beam" mechanism is achieved, with acceptable maximum values of the ductility demand for the columns of all the storeys.

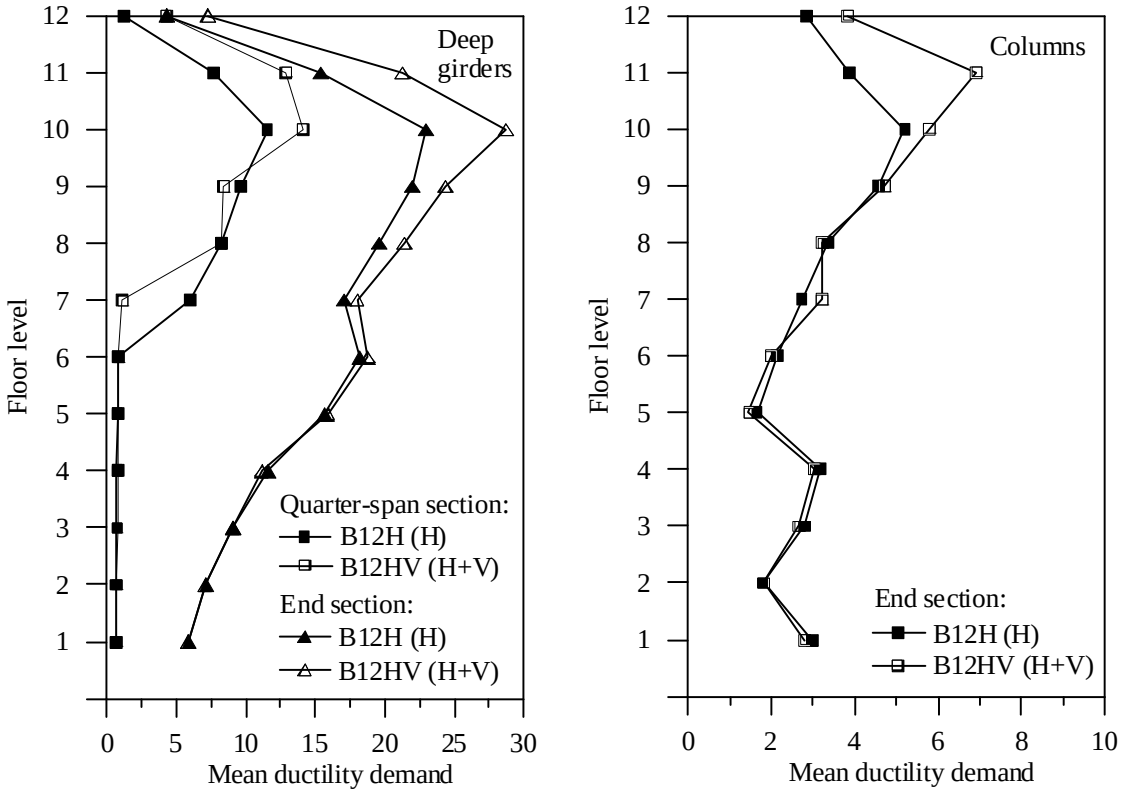

Figure 6: Mean ductility demand of B12H and B12HV structures subjected, respectively, to the horizontal components (H) and horizontal and vertical components (H+V) of the Imperial Valley earthquakes.

Finally, attention was focused on the axial force attained by the columns, in order to check whether failure phenomena occur: i.e. failure under compression or tension, due to the attainment of the corresponding ultimate compressive load, N_{cu}, or tensile load, N_{tu}; brittle failure under a compressive load greater than the balanced load N_b. For this purpose, the minimum (N_{min}) and maximum (N_{max}) values attained by the axial load (assuming positive to be a compressive load) in the corner and central columns of B6H and B6HV structures subjected, respectively, to the horizontal (H) and horizontal and vertical (H+V) components of ECDA ground motion are plotted in Figure 7. Analogous curves are also plotted in Figure 8 with reference to B12H and B12HV structures subjected, respectively, to the H and H+V components of ECA#5 ground motion. As can be observed, the axial-force variation induced a rather high compressive force, which in many columns was greater than the balanced load, thus produc-

ing a reduction in both the ultimate bending moment and available ductility. It should be noted that a compressive load greater than N_b does not necessarily imply a brittle failure, because it depends on the value attained by the bending moment, which may be less than the ultimate moment corresponding to the current axial load. Nevertheless, caution is needed when the compressive load is greater than N_b. It is also useful to note that NTC08 requires that, in the case of medium ductility class, the maximum compressive load for the columns should not be greater than 65% of the corresponding ultimate load N_{cu}.

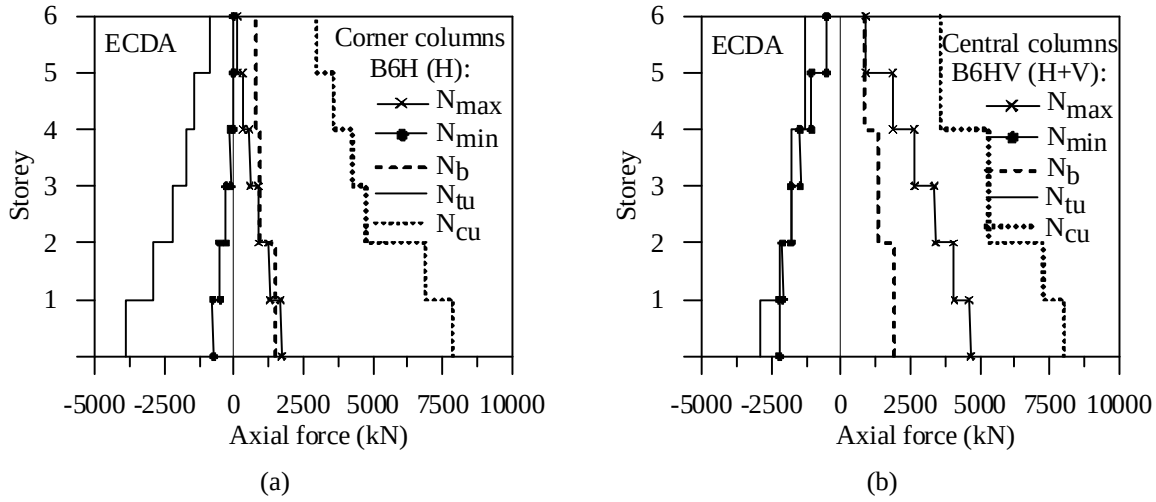

Figure 7: Typical values of column axial forces for the corner and central columns of B6H and B6HV structures subjected to El Centro D.A. records.

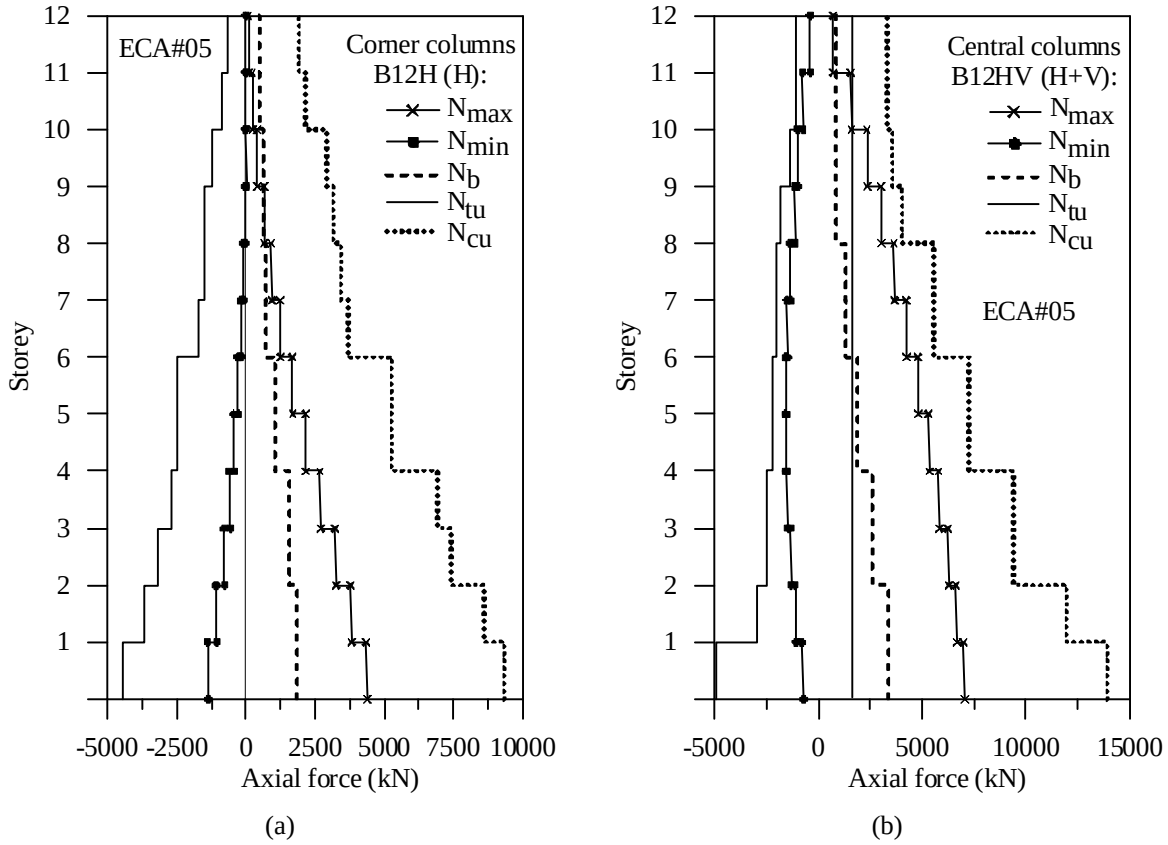

Figure 8: Typical values of column axial forces for the corner and central columns of B12H and B12HV structures subjected to El Centro Array #5 records.

The overturning moment due to the horizontal components of ECDA and ECA#5 ground motions induced an evident variation of the axial load in the corner columns of B6H (Figure 7a) and B12H (Figure 8a) structures. On the other hand, for the central columns, having the greatest tributary mass (i.e. their tributary mass in a storey is about four times the analogous mass corresponding to the corner columns, respectively), the addition of the vertical ground motion produced an evident variation in the axial force giving rise even to a tensile force, which in many sections of B6HV (Figure 7b) and B12HV (Figure 8b) structures is very close to the ultimate tensile force N_{tu}.

5 CONCLUSIONS

An efficient nonlinear beam model based on the Haar–Kàrmàn principle has been proposed for the analysis of r.c. spatial frames subjected to the vertical component of near-fault ground motions. Specifically, the lumped plasticity model for a column (LPMC) includes a piecewise linearization of the bounding surface of the elastic domain corresponding to axial load-biaxial bending moment interaction. A satisfactory compromise between accuracy and computational efficiency has been attained considering 26 flat surfaces: i.e., 6 surfaces normal to the principal axes; 12 surfaces normal to the bisections of the principal planes; 8 surfaces normal to the bisections of the octants. Moreover, the lumped plasticity model for a girder (LPMG) takes into account the potential plastic hinges along the span of the girders, due to the vertical ground motion, modifying the uniaxial plastic moments of the end-sections depending on the top and bottom plastic moments of selected critical intermediate sections. LPMG allowed a reduction in the computational effort due to the sub-discretization of the girders by about 2/3.

Afterwards, a computer code was developed on the basis of the proposed LPMC and LPMG, in order to investigate the effects of the vertical component of near-fault ground motions on the inelastic behavior of r.c. spatial frames. To this end, six- and twelve-storey r.c. framed buildings were designed assuming, besides the gravity loads, the horizontal seismic loads acting alone or in combination with the vertical ones. In order to emphasize the effects due to the vertical component, the numerical investigation was carried out with reference to cases in which the considered horizontal components of the motion acted alone or contemporaneously with the corresponding vertical component. The numerical results showed that the frame members should be designed to also take into account the vertical ground motion. Specifically, the ductility demand increased in many end sections and quarter-span sections of deep girders, while for flat girders it did not depend on the vertical component due to their small tributary mass. As regards the columns, a large variation in the axial force occurred producing even tension (close to the ultimate tensile force) and high compressive forces (larger than the balanced force) which are more evident, respectively, at the upper and lower storeys of the test structures.

ACKNOWLEDGEMENTS

The present work was financed by the Italian Ministry of Education, University and Research.

REFERENCES

[1] A.J. Papazoglou, A.S. Elnashai, Analytical and Field Evidence of the Damaging Effect of Vertical Earthquake Ground Motion. *Earthquake Engineering and Structural Dynamics*, **25**, 1109-1137, 1996.

[2] S.J. Kim, A.S. Elnashai, Seismic assessment of rc structures considering vertical ground motion. University of Illinois at Urbana-Champaign, USA, *MAE Center Report* No. 08-03, 2008.

[3] Technical Regulations for Constructions. *Italian Ministry of the Infrastructures.*2008.

[4] Eurocode 8. Design of structures for earthquake resistance - part 1: general rules, seismic actions and rules for buildings. *UNI ENV 1998-1*, 2003.

[5] S. Li, L.-L. Xie, Progress and trend on near-field problems in civil engineering. *Acta Seismologica Sinica,* 20(1):105-114, 2007.

[6] L. Di Sarno, A.S. Elnashai, G. Manfredi, Effects of vertical earthquake ground motions on rc structures. *14th European Conference on Earthquake Engineering*, Skopije, Republic of Macedonia, CD-ROM, paper No. 289, 2010.

[7] R. Alaghebandian, S. Otani, H. Shiohara, Effect of distributed mass on earthquake response of reinforced concrete frames. *12th World Conference on Earthquake Engineering, Auckland, New Zealand*, paper No. 2230, 2000.

[8] F. Mazza, A. Vulcano, Nonlinear dynamic response of rc framed structures subjected to near-source ground motions: effects of the vertical component. *Fédération Internationale du Béton (FIB), 2nd International Congress*, paper No. 8-24, 2006.

[9] FIB. Practitioners' guide to finite element modeling of reinforced concrete structures. State-of-art report. *FIB Bulletin* No. 45, 2008.

[10] F. Mazza, M. Mazza, Modeling of spatial frames to study the effects of the vertical component of near-fault earthquakes. *14th European Conference on Earthquake Engineering*, Skopije, Republic of Macedonia, paper No. 293, 2010.

[11] F. Mazza, M. Mazza, Nonlinear analysis of spatial framed structures by a lumped plasticity model based on the Haar–Kàrmàn principle. *Computational Mechanics,* **45**, 647-664, 2010.

[12] G.M. Sfakianakis, Biaxial bending with axial force of reinforced, composite and repaired concrete sections of arbitrary shape by fiber model and computer graphics. *Advances in Engineering Software,* **33**, 227-242, 2002.

[13] M. Malena, R. Casciaro, Finite Element Shakedown Analysis of Reinforced Concrete 3D Frames. *Computers and Structures*, **86**, 1176-1188, 2008.

[14] Pacific Earthquake Engineering Research Center database. http://peer.berkeley.edu/smcat/search.html.